

Ultrathin Ag films on H:Si(111)-1×1 surfaces deposited at low temperatures

T. Müller and H. Nienhaus^{a)}

Laboratorium für Festkörperphysik, Gerhard-Mercator-Universität Duisburg, Lotharstrasse 1, 47048 Duisburg, Germany

(Received 23 July 2002; accepted 28 October 2002)

The growth, structure, and electronic properties of thin Ag films on H-terminated Si(111) surfaces were investigated with Auger electron and photoelectron spectroscopy (and atomic force and secondary electron microscopy). The films were either evaporated at room temperature (RT) or deposited at low temperature (LT) and subsequently annealed to RT in the thickness range between 1 and 50 monolayers (0.2–12 nm). The LT preparation leads to large Ag islands on a wetting monolayer which form a continuous Ag film above a critical thickness of 30 monolayers. Ultraviolet photoelectron spectra and work function measurements reveal a (111) surface orientation of the Ag islands. In contrast, RT deposition results in Stranski-Krastanov growth of smaller and irregularly shaped islands which do not form a continuous layer even up to film thicknesses of 45 monolayers.

© 2003 American Institute of Physics. [DOI: 10.1063/1.1530714]

I. INTRODUCTION

The growth of ultrathin metal films on semiconductor surfaces is of fundamental interest as well as of high technological relevance. It affects issues of thin film metallization and the design of electronic devices on the nanometer scale. Recently, large-area metal-semiconductor (Schottky) diodes with metal films in the thickness range of 10 nm were used as detectors for chemically induced hot charge carriers.^{1–4} High sensitivities were achieved with Ag/Si(111) diodes which were fabricated by Ag evaporation on hydrogen-terminated Si(111) substrates at low temperature (LT) and subsequent annealing to room temperature (RT). The corresponding chemicurrent strength is significantly determined by structural properties of the ultrathin Ag film.

The relationship between the morphology of thin Ag films on Si and deposition conditions has been investigated extensively in recent decades. However, few studies are focused on the growth of thin metal films on H-terminated Si surfaces and mostly at substrate temperatures above RT.^{5–20} In a series of papers Oura and co-workers demonstrated a Volmer-Weber growth mode of Ag on H:Si(111) at 600 K leading to flat, single-domain islands with (111) orientation.^{5–7} This quasi-layer-by-layer growth of the islands was recently applied to characterize surface states and Fermi surfaces of thin Ag films by angular resolved photoemission spectroscopy.¹⁴ The different growth of Ag on clean and H-terminated Si(111) surfaces has been attributed to an enhanced surface migration and an increased nucleation site density due to the hydrogen termination.⁵ Depth-resolved measurements of hydrogen using a resonant nuclear reaction revealed that Ag deposition at 360 K leads to out-diffusion of interfacial hydrogen toward the Ag surface.¹³ If the metal is evaporated at 110 K, hydrogen atoms stay at the Ag/Si interface. However, annealing to RT promotes the hydrogen depletion at the interface again. Thus, the altered growth

mode is most likely due to a different reconstruction of the pristine Si-7×7 and the H:Si-1×1 surfaces.

Recently, extremely flat and thin metal films on different semiconductor surfaces were achieved by LT evaporation and subsequent annealing to RT.^{21–28} For H-terminated Si(111) surfaces, little is known about how this technique affects the Ag film growth. Similar studies of Cu evaporation on H:Si(111) demonstrated that the Schottky diode properties are effectively changed during annealing.²⁹ The present study addresses issues of the morphology and electronic properties of LT-deposited and annealed Ag films on H:Si(111)-1×1 which are now routinely used for detection of reactive chemical species.

II. EXPERIMENTAL DETAILS

The samples are cut from *n*-type doped Si(111) wafers with resistivities between 1 and 10 Ω cm. The surfaces are cleaned and terminated with hydrogen atoms by wet-chemical treatments. After subsequent cleaning in ultrasonic baths of acetone, ethanol, and deionized water for 5 min each, the samples are etched in hydrofluoric acid (40%) for 1 min. Two minutes prior to removal of the sample, the etchant is buffered by adding an aqueous solution of HF:NH₄F:NH₄OH until pH=11 to avoid step formation. Eventually, transfer of the H-terminated passivated samples into ultrahigh vacuum (UHV) occurs within 20 min.

Metal deposition and analysis of the surface properties are performed in a UHV double-chamber system at a base pressure of typically 10⁻¹⁰ hPa. Ag films are evaporated on the H:Si(111) surfaces at either RT or low substrate temperature of (210±10) K by use of an effusion cell. The deposition rate is adjusted to approximately 0.01 nm/s. During evaporation the background pressure increases to between 4×10⁻¹⁰ and 2×10⁻⁹ hPa. Samples with Ag films deposited at LT are annealed to RT within 8 h. Throughout this article the metal film thickness is given in monolayers (ML) where 1 ML=0.236 nm, which corresponds to the distance between neighboring Ag(111) planes.

^{a)}Electronic mail: nienhaus@uni-duisburg.de

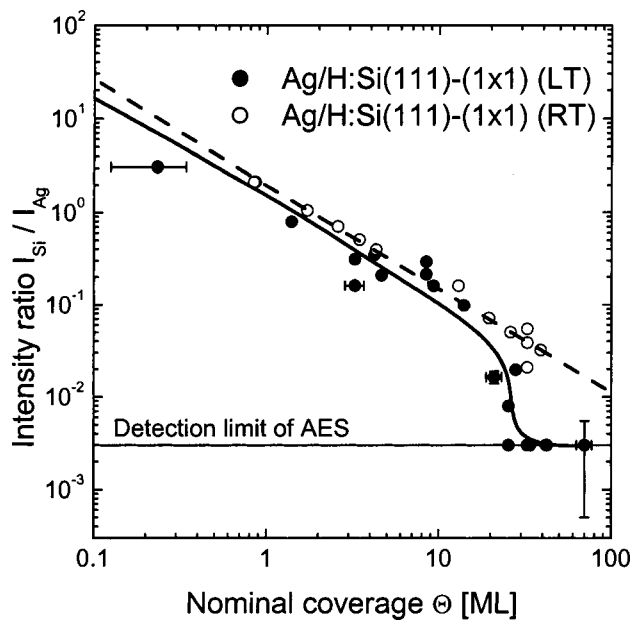


FIG. 1. AES intensity ratio I_{Si}/I_{Ag} as a function of the nominal Ag coverage on H:Si(111). Solid circles: deposition at LT and annealing to RT; open circles: deposition at RT. Above 30 ML at LT deposition, no substrate signal is detected. The dashed line represents a linear fit and the solid line is meant to guide the eye.

The chemical composition of the surface is studied with electron induced Auger electron spectroscopy (AES) with a primary electron energy of 3 keV and high-resolution electron energy-loss spectroscopy (HREELS). The Auger spectra are recorded in the first-derivative mode. They reveal residual carbon and oxygen contaminations of the H-terminated Si(111) surfaces close to the detection limit of the apparatus, i.e., a few percent of a monolayer. HREEL spectra of H:Si(111) surfaces exhibit pronounced features due to Si-H bending and stretching vibrations at loss energies of 80.6 and 259.8 meV, respectively. Low-energy electron diffraction shows bright 1×1 spots of the hydrogen-covered Si surface indicating an excellent hydrogen termination.

The Ag film morphology on the micrometer scale is investigated by secondary electron microscopy (SEM) with electrons of 20 keV and atomic force microscopy (AFM) in tapping mode under ambient atmosphere. Both methods require a transfer of the samples outside UHV. The electronic properties of the surfaces are investigated by ultraviolet photoemission spectroscopy (UPS) with 21.2 eV photons originating from a He I discharge lamp.

III. RESULTS AND DISCUSSION

A. AES results: Ag film growth

To study the growth of Ag films on H-terminated Si(111) surfaces, the ratio of the AES intensities of the Si(LMM) line at 91 eV and the Ag($M_4N_{4,5}N_{4,5}$) feature at 355 eV was measured as a function of the Ag coverage Θ . The data for RT deposition (open circles) and LT deposition with annealing (solid circles) are plotted in Fig. 1 on a double logarithmic scale. The dashed line is a linear fit through the RT data demonstrating a Θ^{-1} dependence of the intensity ratio. The

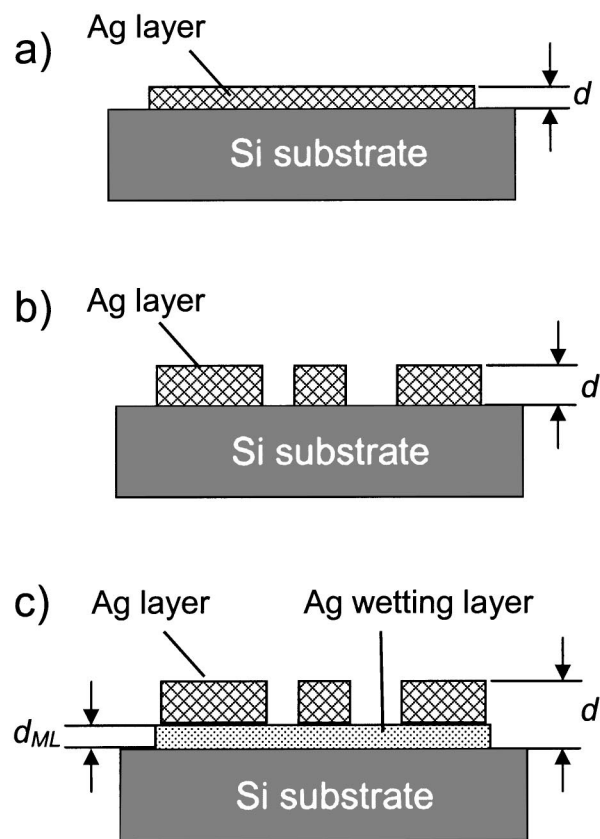


FIG. 2. Different layer models: (a) epitaxial layer-by-layer growth; (b) true island growth; (c) Stranski-Krastanov growth with wetting layer of 1 ML thickness.

LT data obey the same trend up to a coverage $\Theta_c \cong 30$ ML. Beyond, the substrate signal is below the detection limit and the data are placed on the detection limit line in Fig. 1. In addition, the LT intensity ratios are slightly smaller than the corresponding RT values at the same coverage. As explained below, this behavior is typical for metal island growth where LT evaporation and annealing lead obviously to continuous Ag films above Θ_c . In contrast, RT deposition gives open Ag layers which do not cover the Si substrate completely up to the maximum studied coverage of 45 ML.

To elucidate the growth mode, the AES data are calculated within a continuum model. Three different modes depicted in Fig. 2 will be discussed: epitaxial layer-by-layer or Frank-van-der-Merwe growth [Fig. 2(a)], growth of islands of identical height or Volmer-Weber growth [Fig. 2(b)], and the intermediate or Stranski-Krastanov mode, i.e., island growth on a wetting layer of 1 ML [Fig. 2(c)].

In the case of epitaxial layer-by-layer growth as shown in Fig. 2(a), the Auger intensity of the Ag(MNN) line may be expressed as

$$\begin{aligned}
 I_{Ag} &= I_p \sigma_{Ag} \int_0^d \exp[-\xi_{Ag}x] dx \\
 &= I_p \sigma_{Ag} \xi_{Ag}^{-1} (1 - \exp[-\xi_{Ag}d]) \quad (1)
 \end{aligned}$$

where I_p is the primary electron beam intensity, σ_{Ag} is a

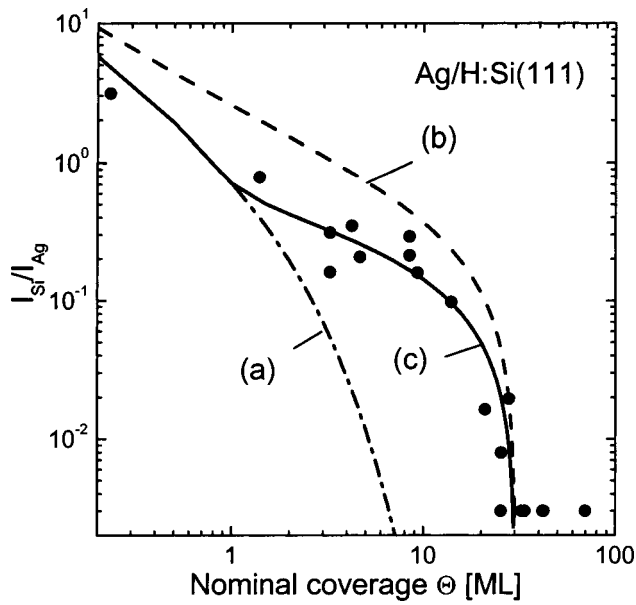


FIG. 3. Calculated Auger intensity ratio I_{Si}/I_{Ag} within the different models of Fig. 2. (a) epitaxial growth; (b) true island growth with $\Theta_c = 30$ ML; (c) Stranski-Krastanov growth with $\Theta_c = 30$ ML. Solid circles: LT data from Fig. 1.

material-dependent factor which includes cross sections, atom densities, and analyzer and sample properties affecting the detection efficiency, and

$$\xi_{Ag} = \left(\frac{1}{\lambda_p} + \frac{1}{\lambda_{Ag} \cos \alpha} \right) \quad (2)$$

contains the energy-dependent, average penetration depths of electrons in matter, which are $\lambda_p(3 \text{ keV}) = 4 \text{ nm}$ and $\lambda_{Ag}(355 \text{ eV}) = 1 \text{ nm}$ for the primary and Ag Auger electrons, respectively.³⁰ In Eq. (2), $\alpha = 43.6^\circ$ denotes the acceptance angle of the cylindrical mirror analyzer so that $\xi_{Ag} = 1.63 \text{ nm}^{-1}$. Likewise, the intensity of the Si(LMM) Auger peak may be written as

$$I_{Si} = I_p \sigma_{Si} \xi_{Si}^{-1} \exp[-\xi_{Si}d]. \quad (3)$$

An escape depth of $\lambda_{Si}(91 \text{ eV}) = 0.45 \text{ nm}$ (Ref. 31) yields $\xi_{Si} = 3.32 \text{ nm}^{-1}$. The film thickness d is proportional to the coverage, i.e., $d = d_{ML}\Theta$ with $d_{ML} = 0.236 \text{ nm}$. Thus, in the case of epitaxial growth, the Auger intensity ratio depends on the Ag film thickness as

$$\left(\frac{I_{Si}}{I_{Ag}} \right)_{\text{epi}} = C \frac{\exp[-\xi_{Si}d]}{1 - \exp[-\xi_{Ag}d]} \quad (4)$$

with the constant $C = \sigma_{Si}\xi_{Ag}/\sigma_{Ag}\xi_{Si}$. The constant C is equal to the Auger intensity ratio of the Si line measured at a pristine Si surface and the Ag line recorded from a thick Ag film. It is measured as $C \approx 0.5$. Expression (4) is plotted as dash-dotted line (a) in Fig. 3 on a double-logarithmic scale. The ratio decreases rapidly with increasing d due to the exponential attenuation of the substrate signal.

The situation is completely different for true island growth as defined in Fig. 2(b). The parameter $\beta = F_{Ag}/F_{\text{tot}}$ measures the ratio between the area of the islands and the total area, i.e., the percentage of the covered Si substrate. We assume that the island area is proportional to the island height d . By introducing the continuous film thickness d_c where $\beta = 1$, it follows that

$$\beta = \begin{cases} d/d_c & \text{for } d \leq d_c, \\ 1 & \text{else.} \end{cases} \quad (5)$$

The relation between d and Θ is now nonlinear since

$$d = \frac{d_{ML}\Theta}{\beta} = \begin{cases} \sqrt{d_{ML}d_c}\Theta & \text{for } d \leq d_c, \\ d_{ML}\Theta & \text{else,} \end{cases} \quad (6)$$

and the Auger intensity of the Ag line may be written as

$$I_{Ag} = \beta I_p \sigma_{Ag} \xi_{Ag}^{-1} (1 - \exp[-\xi_{Ag}d]). \quad (7)$$

The intensity of the Si line consists of two components I_{S1} and I_{S2} from the uncovered and covered substrate areas, according to

$$I_{Si} = I_{S1} + I_{S2} = I_p \sigma_{Si} \xi_{Si}^{-1} \{ (1 - \beta) + \beta \exp[-\xi_{Si}d] \}. \quad (8)$$

The intensity ratio for true island growth obeys the relation

$$\left(\frac{I_{Si}}{I_{Ag}} \right)_{\text{island}} = C \frac{d_c/d + \exp[-\xi_{Si}d] - 1}{1 - \exp[-\xi_{Ag}d]} \quad (9)$$

which is proportional to $1/d$ in the film thickness interval $\xi^{-1} < d < d_c$. In Fig. 3, the corresponding relation is plotted as a dashed line (b) for $\Theta_c = 30$ ML and follows a straight line well below $\Theta_c = d_c/d_{ML}$. At the critical value, when the islands rapidly form a continuous metal layer, the ratio shows a singularity on the logarithmic scale. The measured LT data from Fig. 1 are included in Fig. 3 as solid circles. The qualitative behavior of the data is well described within the island growth model. However, the quantitative agreement is poor. Therefore, Stranski-Krastanov growth is favored to describe the observed variation of the Auger intensities.

For the intermediate growth mode, a wetting layer of 1 ML is assumed as shown in Fig. 2(c). The Auger intensities of the substrate and the metal lines may be decomposed into two summands so that the intensity ratio may be written as

$$\left(\frac{I_{Si}}{I_{Ag}} \right)_{\text{SK}} = C \frac{d/d_c \exp[-\xi_{Si}d] + (1 - d/d_c) \exp[-\xi_{Si}d_{ML}]}{d/d_c (1 - \exp[-\xi_{Ag}d]) + (1 - d/d_c) (1 - \exp[-\xi_{Ag}d_{ML}])} \quad (10)$$

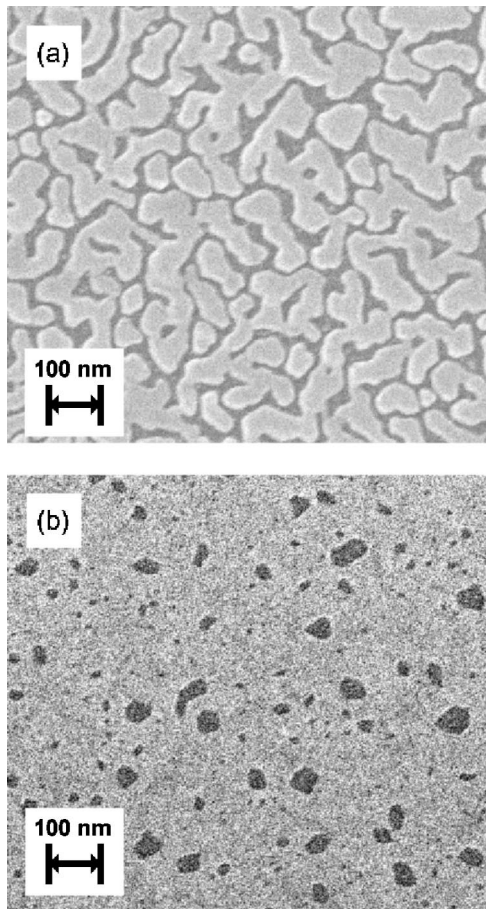


FIG. 4. SEM images of Ag layers on H:Si(111). (a) 42 ML Ag film deposited at RT; (b) 34 ML Ag film deposited at LT and annealed to RT.

in the range $1 \text{ ML} < \Theta \leq \Theta_c$ where the metal thickness and coverage are related by

$$d = d_{\text{ML}} + (\Theta - 1)d_{\text{ML}}/\beta$$

$$= 0.5(d_{\text{ML}} + \sqrt{d_{\text{ML}}^2 + 4d_{\text{ML}}d_c(\Theta - 1)}) \quad (11)$$

with $d_c = d_{\text{ML}}\Theta_c$. For coverages below 1 ML, the ratio obeys Eq. (9) according to true island growth. In Fig. 3, Eq. (10) is plotted as a solid line (c) and is in good agreement with the LT data.

For RT deposition on H:Si(111), the Si substrate signal does not vanish up to Ag film thicknesses of 45 ML. Apparently, the RT growth follows a Stranski-Krastanov behavior as well. Within the model assumptions, the ratio d/β between the thickness of the Ag film and the percentage of area covered by islands is equal to d_c , i.e., increasing values of d_c imply the growth of metal islands of decreasing area and growing height. Thus, RT deposition leads to islands on a wetting layer which are larger in height but smaller in area than for LT evaporation and subsequent annealing.

B. SEM and AFM results: Ag film morphology

The morphology of the films was studied by using SEM and air-ambient AFM for Ag film thicknesses above the continuous film value d_c for LT deposition. The images were taken after transferring the samples out of UHV. In Fig. 4,

two normal-emission SEM images are shown where the top panel [Fig. 4(a)] refers to a 42 ML film deposited at RT on H:Si(111). The Ag layer is composed of partly coalescing metal islands of nonuniform shape very similar to SEM images of Ag films on H:Si(111) reported by others.^{9,12} The islands in Fig. 4(a) cover approximately 78% of the total area. According to the presented growth models, the critical thickness $d_c = d/\beta$ may be estimated as approximately 54 ML. However, inserting this value in Eq. (10) leads to a poor agreement with the RT data, indicating the limitations of the model especially for describing RT growth.

Figure 4(b) shows the SEM image of a 34 ML Ag film deposited at LT and annealed to RT. As expected for Ag layers above Θ_c , the film is continuous. However, a few holes of 20–80 nm in diameter are observed. The depths and origin of the holes are not known but they may be related to substrate contamination which locally affects the layer growth.

AFM was applied to investigate the surface roughness as shown in Fig. 5. The top panel [Fig. 5(a)] shows an image with the corresponding cross-sectional scan of a 30 ML Ag film on H:Si(111) evaporated at RT. The film consists of small irregular islands similar to the pattern of Fig. 4(a). The cross section shows deep valleys in the range of the nominal thickness of 7 nm which are typical for an ultrathin wetting layer. In Fig. 5(b), the results from a 34 ML thick Ag film deposited at LT are presented. Similarly to the RT case, the surface is rough, exhibiting deep valleys, but the islands are more extended and have a circular shape. From SEM it is known that the film is continuous, i.e., the valleys do not expose the Si substrate. The different island distributions are in good qualitative agreement with the AES results which suggested smaller island area/thickness ratios for RT-deposited films than for LT evaporation and annealing.

C. UPS results: electronic properties and orientation of LT Ag films

The electronic properties of thin Ag films deposited at LT on H:Si(111) surfaces and annealed to RT were studied with photoelectron spectroscopy. In Fig. 6, UP spectra for different nominal Ag layer thicknesses are presented. The spectrum at the bottom of the figure was recorded from the uncovered, H-terminated Si(111)- 1×1 surface exhibiting two characteristic Si(111) structures B1 and B2 and an extrinsic surface state (Si-H) at 5.75 eV below the Fermi level.³²

The formation of Ag structures with increasing metal layer thickness is demonstrated in the four top UP spectra in Fig. 6. Electron emission from the Fermi level can be detected for nominal coverages above 1 ML in agreement with the growth model that first a (nonmetallic) wetting layer of 1 ML thickness is formed on which (metallic) islands grow. The same behavior is observed in the development of the three structures Ag1 to Ag3 of the Ag d band. They significantly change position and intensity in the coverage regime around 1 ML when dominant electron emission from metallic Ag bonds starts to exceed emission from Ag-Si bonds. Similar energy shifts have been observed during Ag deposition on Si(111)- 7×7 and Ag:Si(111)- $\sqrt{3} \times \sqrt{3}$ surfaces.³³

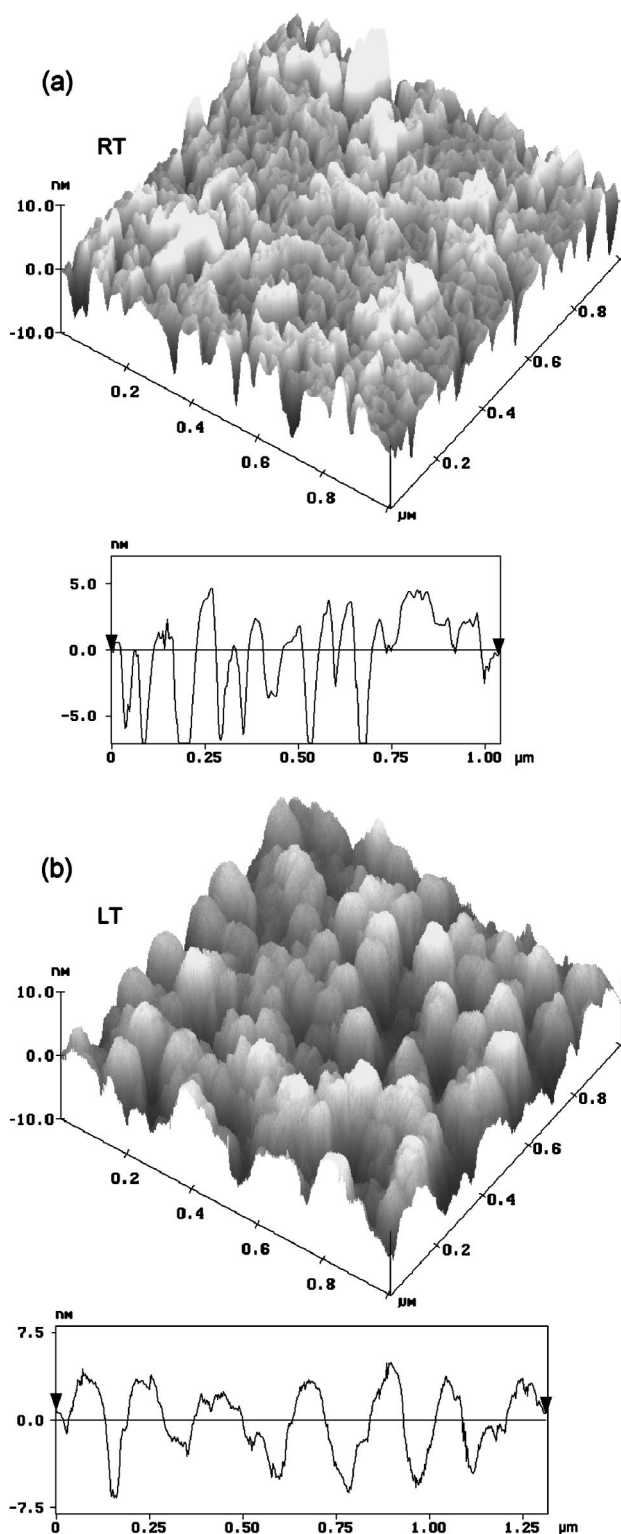


FIG. 5. AFM images and cross sections of Ag layers on H:Si(111) recorded under ambient atmosphere. (a) 30 ML Ag film deposited at RT; (b) 34 ML Ag film deposited at LT and annealed to RT.

Above 1 ML the changes of the spectra in Fig. 6 are only marginal.

The energy position of the three dominating d -band structures in UP spectra recorded with a cylindrical mirror analyzer using He I radiation are dependent on surface orientation. At the top of Fig. 6, the UP line positions are indicated

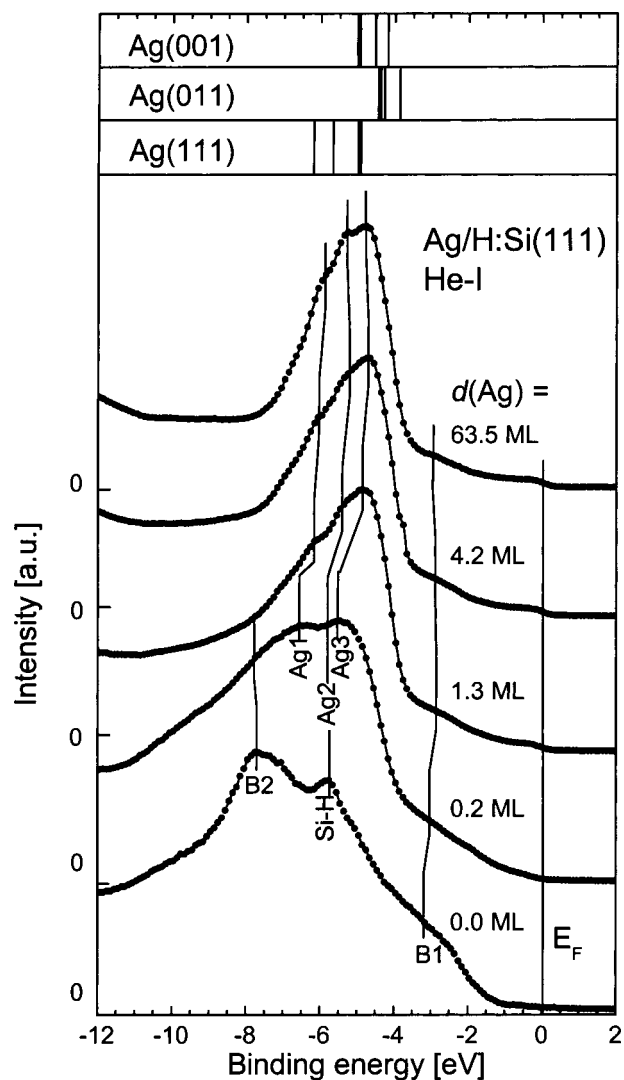


FIG. 6. UP spectra of Ag films on H:Si(111) surfaces recorded with He I photons (21.2 eV). The Ag films were deposited at LT and annealed. The bottom spectrum is recorded from an uncovered surface. The top shows the major Ag d -band features of UP spectra from differently oriented, single-crystalline Ag surfaces (Ref. 34).

for three differently oriented single-crystalline Ag surfaces from Ref. 34. The broader marker lines represent the energy position of the most intense UP structure in each spectrum. The observed features in the measured spectra from thin Ag films on H:Si(111) agree well with results from Ag(111) surfaces, demonstrating the predominantly (111) orientation of the Ag islands.

The variation of the work function Φ as a function of the nominal Ag layer thickness gives additional evidence for the (111) orientation as shown in Fig. 7. The Φ values were obtained by taking the energy difference between the low-energy UP spectrum onset and the Fermi level. The work function of the H-terminated Si(111) surface was measured on a large number of different samples, yielding a value of 4.5 eV. Evaporating extremely thin Ag films at LT and annealing reduces the work function to approximately 4.2 eV which is close to the value of polycrystalline Ag surfaces. The work function increases with film thickness and reaches (4.65 ± 0.15) eV for films above 20 ML. This value is slightly

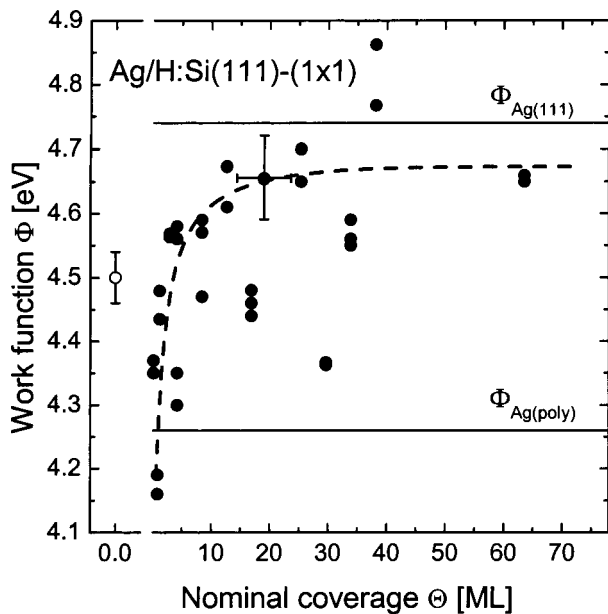


FIG. 7. Variation of work function with nominal Ag film thickness. The Ag films were deposited at LT and annealed to RT. The open circle represents the work function of the H:Si(111) surface. The dashed line is meant to guide the eye and the solid lines show the work functions of single-crystalline Ag(111) and polycrystalline Ag surfaces.

smaller than the work function of single-crystalline Ag(111) surfaces at 4.74 eV.³⁵ The remaining discrepancy may be attributed to the enhanced surface roughness of the films, which is expected to reduce the work function.

LEED images (not shown here) of samples with Ag films above the critical thickness show Ag induced weak spots. In agreement with the concluded (111) orientation of the islands, the spots are arranged hexagonally and exhibit the same azimuthal orientation as the Si(111) substrate.

IV. SUMMARY

The growth and properties of thin Ag films on H-terminated Si(111) were investigated with Auger and photoelectron spectroscopy and atomic force and secondary electron microscopy. The films were either evaporated at RT or deposited at LT (210 K) and subsequently annealed to RT. The growth mode and Ag film quality differ significantly after the two preparation processes. RT and LT deposition followed by annealing lead to island growth on an ultrathin Ag wetting layer. However, the LT-grown and annealed islands are much larger and form a continuous Ag film above a critical thickness of 30 ML. In contrast, the RT films are discontinuous even above nominal coverages of 45 ML and exhibit a complicated and open island structure. From the UP spectra and work function results of LT-deposited Ag layers a predominantly (111) orientation of the islands can be concluded.

ACKNOWLEDGMENTS

The authors thank B. Stahlmecke for providing the SEM images. Financial support by the Deutsche Forschungsgemeinschaft (Contract No. NI469) is gratefully acknowledged.

- ¹H. Nienhaus, Surf. Sci. Rep. **45**, 1 (2002).
- ²B. Gergen, H. Nienhaus, W. H. Weinberg, and E. W. McFarland, Science **294**, 2521 (2001).
- ³H. Nienhaus, H. S. Bergh, B. Gergen, A. Majumdar, W. H. Weinberg, and E. W. McFarland, Appl. Phys. Lett. **74**, 4046 (1999).
- ⁴H. Nienhaus, H. S. Bergh, B. Gergen, A. Majumdar, W. H. Weinberg, and E. W. McFarland, Phys. Rev. Lett. **82**, 446 (1999).
- ⁵K. Sumitomo, T. Kobayashi, F. Shoji, K. Oura, and I. Katayama, Phys. Rev. Lett. **66**, 1193 (1991).
- ⁶M. Naitoh, F. Shoji, and K. Oura, Surf. Sci. **242**, 152 (1991).
- ⁷Y. Ohba, I. Katayama, Y. Yamamoto, M. Watamori, and K. Oura, Appl. Surf. Sci. **113/114**, 448 (1997).
- ⁸R. Naik, C. Kota, B. U. M. Rao, and G. W. Auner, J. Vac. Sci. Technol. A **12**, 1832 (1994).
- ⁹X. B. Zhang, A. L. Vasiliev, G. Van Tendeloo, Y. He, L.-M. Yu, and P. A. Thiry, Surf. Sci. **340**, 317 (1995).
- ¹⁰M. Naitoh, A. Watanabe, and S. Nishigaki, Surf. Sci. **357–358**, 140 (1996).
- ¹¹A. Nishiyama, G. ter Horst, P. M. Zagwijn, G. N. van den Hoven, J. W. M. Frenken, F. Garten, A. R. Schlattmann, and J. Vrijmoeth, Surf. Sci. **350**, 229 (1996).
- ¹²T. Wadayama, O. Suzuki, K. Takeuchi, H. Seki, T. Tanabe, Y. Suzuki, and A. Hatta, Appl. Phys. A: Mater. Sci. Process. **69**, 77 (1999).
- ¹³K. Fukutani, H. Iwai, Y. Murata, and H. Yamashita, Phys. Rev. B **59**, 13 020 (1999).
- ¹⁴A. Arranz, J. F. Sánchez-Royo, J. Avila, V. Pérez-Dieste, P. Dumas, and M. C. Asensio, Phys. Rev. B **65**, 075405 (2002).
- ¹⁵B. Gergen, H. Nienhaus, W. H. Weinberg, and E. W. McFarland, J. Vac. Sci. Technol. B **18**, 2401 (2000).
- ¹⁶I. Matsuda, H. W. Yeom, T. Tanikawa, K. Tono, T. Nagao, S. Hasegawa, and T. Ohta, Phys. Rev. B **63**, 125325 (2001).
- ¹⁷T. Fujino, T. Okuno, M. Katayama, and K. Oura, Jpn. J. Appl. Phys., Part 2 **40**, L1173 (2001).
- ¹⁸K. Oura, V. G. Lifshits, A. A. Saranin, A. V. Zotov, and M. Katayama, Surf. Sci. Rep. **35**, 1 (1999).
- ¹⁹J.-T. Ryu, O. Kubo, H. Tani, T. Harada, M. Katayama, and K. Oura, Surf. Sci. **433–435**, 575 (1999).
- ²⁰J.-T. Ryu, K. Kui, K. Noda, M. Katayama, and K. Oura, Surf. Sci. **401**, L425 (1998).
- ²¹Z. Zhang, Q. Niu, and C.-K. Shih, Phys. Rev. Lett. **80**, 5381 (1998).
- ²²A. R. Smith, K.-J. Chao, Q. Niu, and C.-K. Shih, Science **273**, 226 (1996).
- ²³K.-J. Chao, Z. Zhang, Ph. Ebert, and C. K. Shih, Phys. Rev. B **60**, 4988 (1999).
- ²⁴L. Huang, S. J. Chey, and J. H. Weaver, Surf. Sci. **416**, L1101 (1998).
- ²⁵M. Horn-von Hoegen, T. Schmidt, M. Henzler, G. Meyer, D. Winau, and K. H. Rieder, Surf. Sci. **331–333**, 575 (1995).
- ²⁶S. Fölsch, G. Meyer, D. Winau, K. H. Rieder, M. Horn-von Hoegen, T. Schmidt, and M. Henzler, Phys. Rev. B **52**, 13 745 (1995).
- ²⁷D. A. Evans, M. Alonso, R. Cimino, and K. Horn, Phys. Rev. Lett. **70**, 3483 (1993).
- ²⁸G. Neuhold and K. Horn, Phys. Rev. Lett. **78**, 1327 (1997).
- ²⁹H. Nienhaus, H. S. Bergh, B. Gergen, A. Majumdar, W. H. Weinberg, and E. W. McFarland, J. Vac. Sci. Technol. A **17**, 1683 (1999).
- ³⁰G. A. Somorjai, *Chemistry in Two Dimensions* (Cornell University Press, Ithaca, NY, 1981).
- ³¹W. Mönch, *Semiconductor Surfaces and Interfaces*, 3rd ed. (Springer, Berlin, 2001).
- ³²Y. He, S. Bouzidi, B.-Y. Han, L.-M. Yu, P. A. Thiry, R. Caudano, and J.-M. Debever, Phys. Rev. B **54**, 17 654 (1996).
- ³³F. Wehking, H. Beckermann, and R. Neddermeyer, Thin Solid Films **36**, 265 (1976).
- ³⁴H. F. Roloff and H. Neddermeyer, Solid State Commun. **21**, 561 (1977).
- ³⁵*Handbook of Chemistry and Physics*, 76th ed., edited by D. R. Lide (CRC Press, Boca Raton, FL, 1996).